Identification of a lipid-rich depot in the orbital cavity of the 13-lined ground squirrel

Amanda D V MacCannell[1,4,*], Kevin J Sinclair[2], Glenn J Tattersall[3], Charles A McKenzie[2] and James F Staples[1]

[1] Dept. of Biology, University of Western Ontario, London ON, N6A5B8, CANADA
[2] Dept. of Medical Biophysics, University of Western Ontario, London ON, N6A5B7, CANADA
[3] Dept. of Biological Sciences, Brock University, St. Catharines ON, L2S3A1, CANADA
[4] Discovery and Translational Science Dept., University of Leeds, Leeds, LS2 9DA, UNITED KINGDOM

* Author for correspondence (umamc@leeds.ac.uk)

Accepted for publication in the Journal of Experimental Biology, January 16, 2019

ABSTRACT

We discovered a previously undescribed orbital lipid depot in the 13-lined ground squirrel during the first ever magnetic resonance image (MRI) of this common experimental model of mammalian hibernation. In animals housed at constant ambient temperatures (5ºC or 25ºC, 12h L:12h D photoperiod) the volume of this depot increased in the autumn and decreased in the spring, suggesting an endogenous circannual pattern. Water-fat MRI revealed that throughout the year this depot is composed of ~40% lipid, similar to brown adipose tissue (BAT). During arousal from torpor, thermal images showed higher surface temperatures near this depot before the rest of the head warmed, suggesting a thermoregulatory function. This depot, however, does not contain uncoupling protein 1, a BAT biomarker, or uncoupling protein 3. Histology shows blood vessels in close proximity to each other, suggesting it may serve as a vascular rete, perhaps to preferentially warm the eye and brain during arousals.

KEY WORDS: (5)

MRI, Hibernation, Adipose, Rete, Lipid, Orbit

INTRODUCTION

The 13-lined ground squirrel (*Ictidomys tridecemlineatus*) is a model organism for investigations of metabolic challenges that face hibernating mammals. The first published Magnetic Resonance Image (MRI) of the 13-lined ground squirrel revealed the novel discovery of what appears to be a substantial depot of fatty tissue in the orbital cavity, located behind the eyes (MacCannell et al., 2017). We imaged this orbital lipid depot using the MRI pulse sequence, ***I***terative ***De***composition of water and fat with ***E***cho ***A***symmetry and ***L***east-squares estimation (IDEAL) which quantifies the proton density fat fraction (PDFF), the fraction of tissue that is composed of lipid (Fuller et al., 2006; Reeder et al., 2005). The PDFF of brown adipose tissue (BAT) is known to be 30 – 70% (Hu et al., 2010; Rasmussen et al., 2013; Prakash et al., 2016) which is lower than that of white adipose tissue (WAT) (80 – 100%). We measured PDFF values of approximately 40% in this newly identified orbital depot (MacCannell et al., 2017).

We initially hypothesized that this lipid depot was one of several glands known to be located behind the eyes of other mammals, especially the Harderian gland (Wei Li, personal communication). In mice, lipid comprises approximately 35% of wet mass of the Harderian (Watanabe, 1980), close to the PDFF values we determined for this depot in ground squirrels. However our preliminary investigations did not detect any porphyrin, a hallmark of the Harderian gland (Kennedy, 1970; Payne, 1994), within this orbital lipid depot. Moreover, we subsequently located the much smaller Harderian gland at the base of the optic nerve and confirmed its identity with a porphyrin assay. By contrast this newly identified orbital lipid depot surrounds the optic nerve just posterior to the eye, and its nature remained unknown.

The PDFF values of this orbital lipid depot also closely resembles that of thorax BAT in ground squirrels (MacCannell et al., 2017). BAT has thermogenic capacity through the futile cycling of the electron transport system (ETS) caused by expression of uncoupling protein 1

(UCP1) which, when activated, allows protons pumped to the mitochondrial intermembrane space by the ETS to re-enter the mitochondrial matrix. In eutherian mammals, UCP1 is expressed predominately, if not exclusively, in BAT (Laursen et al., 2015), whereas other proteins in this family, such as UCP3, are expressed predominately in muscle (Raimbault et al., 2001). Due to the MRI characteristics of this orbital lipid depot we speculated that it might indeed be a BAT depot. Data from other mammalian hibernators supported this idea. Thermal images of hibernating bears show higher temperature around the eyes than the rest of the head (Laske et al., 2010). Also, Arctic ground squirrels (*Spermophilus parryii*) housed at -10°C showed a significantly higher brain temperature, compared with liver, rectum, WAT and gastrocnemius muscle (Barger et al., 2006).

Hibernators have adapted to the thermal and energetic challenges of winter by undergoing seasonal hibernation, a strategy characterized by bouts of torpor that are spontaneously interrupted by periods of interbout euthermia (IBE). In Richardson's ground squirrels (*Urocitellus richardsonii*) entrance into torpor involves suppression of whole-animal metabolic rate, heart rate, and body temperature (T_b) by 90%, 100-fold, and 32°C, respectively (Wang, 1979). During arousal from torpor, BAT is activated, increasing both metabolic rate and T_b. In most mammals, including the 13-lined ground squirrel (MacCannell et al., 2017; MacCannell et al., 2018a), BAT is located predominately within the thorax. We predict that, if this orbital lipid depot is indeed BAT then areas of the head near it may be warmer than other areas distal to thorax BAT depots during arousal. In most eutherian mammals, growth of BAT requires several days of exposure to decreased ambient temperature (T_a) (Nakamura and Morrison, 2007) or high-calorie diets (Rothwell and Stock, 1979). In hibernators, however, we (MacCannell et al., 2018a) and others (Hindle and Martin, 2014) have found indications that BAT depots increase in size in the late summer and early autumn without cold exposure,

suggesting regulation by an endogenous rhythm. If this cranial depot is indeed BAT, then we predict that it would show a similar pattern of growth to thoracic BAT and would express UCP1.

To our knowledge our study (MacCannell et al. 2017) was the first to describe this orbital lipid depot, and there is no information about its properties or potential relevance for a hibernator. In this study we endeavoured to explore the structural and biochemical properties of this orbital lipid depot as well as its seasonal dynamics.

MATERIALS AND METHODS

Experimental Animals

All procedures were approved by the University of Western Ontario Animal Care Committee (protocol 2012-016) and followed Canadian Council on Animal Care guidelines. Details of ground squirrel trapping and husbandry followed those we published recently (MacCannell et al., 2017).

For the MRI experiments we used juvenile male ground squirrels from the same litter that were housed at 22°C until weaning, after which they were divided randomly into two conditions: (n=4 for each): cold-housed (5°C) or warm-housed (thermoneutral; 25°C). After the initial MRI scan (see following section) of the cold-housed squirrels on 19 August 2016 the ambient temperature was decreased 1°C/day until ambient temperature reached 5°C (6 September 2016). On 26 August 2016, immediately after the first MRI scan of the warm-housed animals, ambient temperature was increased to 25°C. Both groups had a 12h Light (L):12h Dark (D) photoperiod. Rat chow (LabDiet 5P00), dry dog food (Iams), and water were provided *ad libitum*, with sunflower seeds and corn provided three times each week. Animals were weighed approximately once per week during cage changes, if animals were in torpor cages were not changed to minimize disturbance. Torpor bouts were confirmed by the sawdust technique (Pengelley and

Fisher, 1961), in which sawdust is placed on the back of a torpid squirrel and animals were observed daily for the presence of the sawdust. We use this technique because instrumenting these animals with T_b telemeters would have interfered with MRI.

Another group of squirrels that hibernated regularly, were used for thermal imaging (see below). These animals were maintained at 22°C during the spring and summer (March until October) while during the winter months these animals were housed at 5°C. Details for housing can be found in Mathers et al., (2017).

MRI Scanning

MRI was used to obtain T1-weighted images and IDEAL water-fat images from both warm-housed and cold-housed animals approximately every three weeks under isoflurane anaesthesia. The two treatment groups (cold and warm-housed) were scanned on alternating weeks. MRI scanning details can be found in our recent publication (MacCannell et al., 2017; MacCannell et al., 2018a).

Segmentation of MR Images

Orbital lipid volume was segmented (i.e. outlined) using the OsiriX 5.6 (Bernex, Switzerland) 2D threshold region-growing algorithm tool with segmentation parameters set to a lower threshold of 30% PDFF and an upper threshold of 70%, i.e. a minimum of 30% and a maximum of 70% of the tissue volume consisted of lipid, based on segmentation guidelines adapted from earlier studies on BAT from mice, rats, and humans (Hu et al., 2010; Prakash et al., 2016; Rasmussen et al., 2013).

Immunoblot Analysis

Both cold-housed and warm-housed animals were euthanized by anaesthetic overdose (Euthanyl, 54 mg/100 g) following the final MRI scan, one year after the initial scan. Thorax BAT, orbital lipid depot, heart, gastrocnemius muscle and forebrain were dissected and stored at -80°C. These

samples were homogenized in Radioimmunoprecipitation assay buffer (RIPA; 50 mM Tris, 150 mM NaCl, 1% SDS, 0.5% sodium deoxycholate and 1% Triton X) for total protein extraction. Samples were centrifuged at 4°C and 10,000 *g* for 20 min before being stored at -80°C. Thirty µg of protein was separated by electrophoresis using 10% sodium dodecyl sulfate-polyacrylamide gels. Gels were run at 180 V for 1 h in a running buffer (25 mM Tris, 190 mM glycine, 0.1% SDS), then transferred to polyvinylidene fluoride membranes. Transfer was conducted at 4°C at 100 V for 2 h. After transfer, membranes were blocked with 5% bovine serum albumin in Tris-buffered saline and Tween-20 (TBST; 30 mM Tris, 137 mM NaCl, 0.1% Tween-20, pH 7.6) under steady agitation for 2 h. Membranes were probed with a rabbit UCP1 antibody (primary-antibody 1:1000; Abcam ab10983) or UCP3 primary antibody (1:1000 in TBST; Abcam, ab10985) overnight at 4°C. Rabbit anti-goat secondary (1:20000; Abcam ab205718) was incubated for 1 h at room temperature under steady agitation. The membrane was washed three times for 10 min each in Tris-buffered saline and Tween-20 (TBST). Bands were visualized using Luminata Forte ECL (Millipore) using a VersaDoc MP5000 imaging system (BioRad). Bands were quantified using the densitometry analysis tool in ImageLab 3.0 (BioRad) and standardized to total protein in each lane, determined using Amido Black staining.

Statistical Analyses

All values are presented as mean ± standard error of the mean (S.E.M.). The effect of time, temperature or interaction of time and temperature on PDFF or orbital lipid depot volume of cold and warm-housed animal were made using a repeated measures ANOVA and Greenhouse-Geisser Correction on SPSS (IBM Corp. Released 2013. IBM SPSS Statistics for Windows, Version 22.0. Armonk, NY: IBM Corp.). Reliability of MRI segmentation volumes was confirmed by calculation of the interclass correlation coefficient (ICC) between values

136 determined by ADVM and a second reader (Prasiddha Parthasarathy); ICC values higher than
137 0.9 indicate excellent reliability (Koo and Li, 2016).

138 **CryoViz Imaging**

139 We used the CryoViz system to obtain visual images of this orbital lipid depot to confirm its
140 corresponding position with MRI scans, and compare it visually with other tissues. One
141 hibernating animal from a separate cohort (housed at 5°C, photoperiod 2h L:22h D) was
142 euthanized by anaesthetic overdose 29 November 2016 (Euthanyl, 54 mg/100 g) immediately
143 following an IDEAL MRI. The squirrel was flash frozen in Optimal Cutting Temperature (OCT)
144 freezing medium (Tissue-Tek® O.C.T. Compound, Sakura® Finetek) by liquid nitrogen
145 immersion. The squirrel was sectioned sagitally every 50 μm and optical images were obtained
146 using a cryo-fluorescence imager (CryoViz^{TM}; Bioinvision, Inc., Cleveland, OH). Block-face
147 images were collected with an in-plane resolution of 10.5×10.5 μm^2. Brightfield images were
148 acquired, stitched together and visualized using proprietary software (Bioinvision, Inc).

149 **Histology**

150 We conducted histology on BAT, orbital fat, and WAT from cold and warm-housed 13-lined
151 ground squirrels. Tissues were removed immediately after sacrificing the animals and placed in
152 10% Formalin for 24 h and then transferred to 70% ethanol until samples could be processed.
153 Tissues were processed and embedded in paraffin wax blocks with a Leica ASP300 fully
154 enclosed tissue processor. Hematoxylin and Eosin (H & E) stain was applied using a Leica
155 Autostainer XL. Tissues were processed and stained at the Western University Robarts
156 Molecular Pathology Core Facility.

157 Imaging of the slides was conducted at the Biotron Integrated Microscopy, Western
158 University using a Zeiss Axioimager Z1 Upright Fluorescent/Compound microscope.

159 **Thermal Imaging**

Animals were removed from their cages to a lighted room and placed into a plastic container inside a small Styrofoam box, that was cooled with icepacks, producing a T_a of approximately 7°C. Thermal imaging began within 1 min of removal of the cage from the environment chamber. We induced arousal in 15 torpid ground squirrels that were hibernating at 5°C, 2h L:22h D photoperiod, by gentle agitation to their feet while in the Styrofoam container. We measured the surface temperature of these animals at 10 sec intervals using a portable infrared thermal camera (Model 7515; Mikron Instruments®, Oakland, HJ, USA). Under these conditions, arousal to voluntary animal movement took, on average, 120 minutes, similar to the time course of spontaneous arousals in this species (MacCannell et al., 2018b). To account for incident radiation, emissivity was set to 0.95 and the appropriate air temperature used as the reflected temperature (reviewed in Tattersall, 2016). Thermal images were analyzed using commercial software (MikroSpec RT®; Mikron Instruments ®).

RESULTS/DISCUSSION

The PDFF of the orbital lipid depot was 40.9±0.5%, indistinguishable from that of BAT with a PDFF of 39.5±0.5% (Figure 1A). The CryoViz images correspond the tissue used in biochemical analysis with the identified orbital lipid depot from the MRI (Figure 1A). Visually this orbital lipid depot also resembles BAT quite closely (Figure 1A). Despite these apparent similarities between the orbital lipid depot and BAT, immunoblots did not detect any UCP1 in the orbital lipid depot (Figure 1B), so the orbital lipid depot cannot be considered BAT. We did detect UCP1 in thoracic BAT, demonstrating strong reactivity with the rabbit-derived antibody. Moreover we did not detect any UCP3 in the orbital lipid depot (Figure 1B), or in heart or BAT, typical for these tissues (Raimbault et al., 2001). The lack of either UCP1 or UCP3 likely rules out any uncoupling thermogenic role for this orbital lipid depot. In recent years the potential for

non-shivering thermogenesis by skeletal muscle has received increasing research interest (reviewed by Rowland et al., 2015). While this possibility is intriguing, the lack of UCP3 suggests that the orbital lipid does not originate from skeletal muscle (Boss et al., 1997), whereas ground squirrel skeletal muscle does show UCP3 reactivity (Figure 1B).

Although we did not detect any potential for uncoupled thermogenesis in the orbital lipid depot, thermal images collected during arousals did show higher surface temperatures for the region near the eye and ear than other parts of the head and thorax, suggesting greater heat loss in the head than thorax (Figure 1C). Using these thermal images, we found that that the surface temperature near the eye increases at a higher rate than the thorax and feet (Supplemental Movie 1; Supplemental Figure 1). The high surface temperature observed around the eyes indicates that this area is losing heat. This heat loss could be caused by lack of insulation or warm blood flowing to this area. Other fat depots, including white adipose tissue (WAT) are good insulators (Trayhurn and Beattie, 2001) and would reduce the rate of heat conduction to the external environment. The high heat loss leads us to believe that this orbital lipid depot is not functioning as an insulator.

The volume of the orbital lipid depot is dynamic, appearing to exhibit a circannual rhythm. Animals used in MRI experiments were housed under warm or cold conditions but under the same 12h L:12h D photoperiod. This design eliminated any overt seasonality cues within each group. Nonetheless there was a significant effect of time ($F_{(3.0, 18.2)}$=10.9, P<0.001), but not ambient temperature ($F_{(1, 6)}$=1.7, P=0.3) on the volume of the orbital lipid depot. The orbital lipid depot of animals housed in constant cold and warm conditions started at 0.16±0.0 ml in late August but increased in size by a factor of 3.3 in both groups by early November (Figure 2A). The depot size plateaued at 0.47±0.0 ml from November until early February before a 2-fold decrease where the depot volume again levelled off at 0.25±0.0 ml in May. After a full year,

the orbital depot was 0.36±0.0 ml in both groups, 2.3-fold greater than the original volume in August 2016. The PDFF of the orbital lipid depot did not vary significantly over time or between the two groups ($F_{(2.6, 15.5)}$=1.5, P=0.26), remaining fairly constant near 43% (Figure 2B). The consistent PDFF indicated that there is no change in the water to fat ratio of the depot despite the changes in depot volume. If this orbital lipid depot was one of the glands commonly found near mammal eyes (Harderian, Meibomian, or lacrimal), we cannot conceive of a hypothesis that would address why its volume would vary 3-fold over the course of a year. Indeed in rats, the mass of the lacrimal gland, located within the orbit, increases linearly following birth, but plateaus at an age of 100 days, without further dramatic changes in size over the lifetime of the animal (Walker, 1958).

Hematoxylin & Eosin staining of BAT showed the well-documented pattern of multivacuolated lipid droplets, while WAT showed univacuolated lipid droplets, typical for these tissues (George, J.C. and Eapen, J., 1959). In contrast, the orbital lipid depot appears to have multi-layered cuboidal epithelial cells surrounding what resemble blood vessels. These distinct patterns allow us to conclude that the eye fat depot does not consist of WAT or BAT. In fact, the presence of blood vessels in close apposition is reminiscent of a vascular rete. H & E staining of a swine *rete mirabile* located at the skull base within the cavernous sinuses, shows similarities to the ground squirrel orbital lipid depot in both cell type, size, and proximity of blood vessels (Arakawa et al., 2007).

The dynamic volume changes, increased regional temperature, lack of UCPs, and high level of vascularization leads us to hypothesize that this tissue might be a rete, a network of many arterial and venous blood vessels in close proximity to each other, creating a counter current pattern of blood flow (Cech et al., 1984). Such structures are found within several different taxa including birds, fish, and mammals, with some retia located near the eyes and

orbital sinuses of salmon sharks and bigeye thresher shark, where they appear to function as vascular heat exchangers (Cech et al., 1984; Weng and Block, 2004). In these animals, such counter current heat exchange restricts heat loss across the surface of the eyes, while presumably warming the nearby brain. Such a mechanism may have been advantageous during the evolution of hibernators such as 13-lined ground squirrels. In this species, hibernation occurs in burrows below the frost line. These animals arouse from torpor spontaneously approximately every 12 days throughout the winter. During arousal metabolic rate and ventilation rate increases substantially (Wang, 1979). The increased rate of intake of cold air through the nasal cavities during arousal could constrain the rate at which the nearby eyes and brain could rewarm, and there is little insulation in this region. Most of the heat generated during the early stages of an arousal is derived from BAT, but BAT is concentrated deep within the thorax, and this heat is delivered convectively to other body regions through the blood. In fact during the early stages of arousal in hamsters blood flow is restricted to the thorax and head (Osborne et al., 2005). As this warm blood reaches the periphery of the head, a rete would reduce loss of heat from warmed blood to the environment through this poorly insulated region. This suggestion is supported by our thermal images; the increase in temperature observed around the eyes could result from warm blood flowing from the thorax and being retained in the region by the rete. The brain plays a major role in regulating changes to T_b, metabolism, and several physiological variables during arousal in other hibernators including the golden-mantled ground squirrel (Heller and Colliver, 1974; Dark et al., 1990), so rewarming of the brain before other tissues would likely be advantageous. To our knowledge, however, such an orbital lipid depot has not been reported in other hibernators, but brain temperature is higher during torpor at a T_a of -10°C in Arctic ground squirrels (Barger et al., 2006), and Columbia ground squirrels warm up their brains before their

body after return to normoxia from hypoxia (Tattersall and Milsom, 2009). Both of these observations could be explained by a rete acting as a head specific heat retention organ.

To confirm that this orbital lipid depot is a *rete mirable*, a "wonderful network" of blood vessels, we propose using the powerful technique of differential-contrast, dual-vascular injection (DICOM) with X-ray microcomputed tomography (micro CT). This method has been used recently to characterize sites of heat exchange within bird heads (Porter and Witmer, 2016). If confirmed this discovery would be the first ever documented rete in the orbital cavity of a mammal, to our knowledge.

Acknowledgements

We thank Lauren Smith and Stephanie Giza for MRI scanning assistance. We thank Prasiddah Parthasarathy for being a second reader for MRIs and Alirezaa Akbari for assistance with reconstruction of MRIs. We thank the University of Western Ontario Biotron for use of microscope, training and support. Also, Robarts pathology lab for histology, Christopher Guglielmo for input and ideas on this project and Amanda Hamilton for help with the CryoViz. We thank Kate Mathers, Leah Hayward and Xingyi Wang for their animal care support.

Competing Interests

The authors declare no competing interests.

Funding

This research was supported by Discovery Grants from the Natural Sciences and Engineering Research Council (Canada) (CAM; RGPIN-2013-356310; GJT; RGPIN-2014-05814, JFS;

278 RGPIN-2014-04860), the Faculty of Science, University of Western Ontario and the Canada
279 Research Chairs program (CAM; 950-228038).

280

REFERENCES

281 **Arakawa, H., Murayama, Y., Davis, C. R., Howard, D. L., Baumgardner, W. L., Marks, M.**
282 **P. and Do, H. M.** (2007). Endovascular Embolization of the Swine Rete Mirabile with
283 Eudragit-E 100 Polymer. *Am. J. Neuroradiol.* **28**, 1191–1196.

284 **Barger, J. L., Barnes, B. M. and Boyer, B. B.** (2006). Regulation of UCP1 and UCP3 in arctic
285 ground squirrels and relation with mitochondrial proton leak. *J. Appl. Physiol.* **101**, 339–
286 347.

287 **Boss, O., Samec, S., Paoloni-Giacobino, A., Rossier, C., Dulloo, A., Seydoux, J., Muzzin, P.**
288 **and Giacobino, J. P.** (1997). Uncoupling protein-3: a new member of the mitochondrial
289 carrier family with tissue-specific expression. *FEBS Lett.* **408**, 39–42.

290 **Cech, J. J., Laurs, R. M. and Graham, J. B.** (1984). Temperature-Induced Changes in Blood
291 Gas Equilibria in the Albacore, Thunnus Alalunga, a Warm-Bodied Tuna. *J. Exp. Biol.*
292 **109**, 21–34.

293 **Dark, J., Kilduff, T. S., Heller, H. C., Licht, P. and Zucker, I.** (1990). Suprachiasmatic nuclei
294 influence hibernation rhythms of golden-mantled ground squirrels. *Brain Res.* **509**, 111–
295 118.

296 **Fuller, S., Reeder, S., Shimakawa, A., Yu, H., Johnson, J., Beaulieu, C. and Gold, G. E.**
297 (2006). Iterative Decomposition of Water and Fat with Echo Asymmetry and Least-
298 Squares Estimation (IDEAL) Fast Spin-Echo Imaging of the Ankle: Initial Clinical
299 Experience. *Am. J. Roentgenol.* **187**, 1442–1447.

300 **George, J.C. and Eapen, J.** (1959). A Histological and Histochemical Study of the Brown and
301 Yellow Adipose Tissue of the Bat, Hipposideros speoris. *J. Cell Sci.* **51**, 369–375.

302 **Heller, H. C. and Colliver, G. W.** (1974). CNS regulation of body temperature during
303 hibernation. *Am. J. Physiol. Leg. Content* **227**, 583–589.

304 **Hindle, A. G. and Martin, S. L.** (2014). Intrinsic circannual regulation of brown adipose tissue
305 form and function in tune with hibernation. *Am. J. Physiol.-Endocrinol. Metab.* **306**,
306 E284–E299.

307 **Hu, H. H., Smith, D. L., Nayak, K. S., Goran, M. I. and Nagy, T. R.** (2010). Identification of
308 Brown Adipose Tissue in Mice with Fat-Water IDEAL-MRI. *J. Magn. Reson. Imaging*
309 *JMRI* **31**, 1195–1202.

310 **Kennedy, G. Y.** (1970). Harderoporphyrin: a new porphyrin from the Harderian glands of the
311 rat. *Comp. Biochem. Physiol.* **36**, 21–36.

Koo, T. K. and Li, M. Y. (2016). A Guideline of Selecting and Reporting Intraclass Correlation Coefficients for Reliability Research. *J. Chiropr. Med.* **15**, 155–163.

Laske, T. G., Harlow, H. J., Garshelis, D. L. and Iaizzo, P. A. (2010). Extreme respiratory sinus arrhythmia enables overwintering black bear survival--physiological insights and applications to human medicine. *J Cardiovasc. Transl. Res.* **3**, 559–569.

Laursen, W. J., Mastrotto, M., Pesta, D., Funk, O. H., Goodman, J. B., Merriman, D. K., Ingolia, N., Shulman, G. I., Bagriantsev, S. N. and Gracheva, E. O. (2015). Neuronal UCP1 expression suggests a mechanism for local thermogenesis during hibernation. *Proc. Natl. Acad. Sci. U. S. A.* **112**, 1607–1612.

MacCannell, A., Sinclair, K., Friesen-Waldner, L., McKenzie, C. A. and Staples, J. F. (2017). Water–fat MRI in a hibernator reveals seasonal growth of white and brown adipose tissue without cold exposure. *J. Comp. Physiol. B* **187**, 759–767.

MacCannell, A. D. V., Sinclair, K. J., McKenzie, C. A. and Staples, J. F. (2018a). Environmental temperature effects on adipose tissue growth in a hibernator. *J. Exp. Biol.* jeb.194548.

MacCannell, A. D. V., Jackson, E. C., Mathers, K. E. and Staples, J. F. (2018b). An improved method for detecting torpor entrance and arousal in a mammalian hibernator using heart rate data. *J. Exp. Biol.* **221**, jeb174508.

Mathers, K. E., McFarlane, S. V., Zhao, L. and Staples, J. F. (2017). Regulation of mitochondrial metabolism during hibernation by reversible suppression of electron transport system enzymes. *J. Comp. Physiol. [B]* **187**, 227–234.

Nakamura, K. and Morrison, S. F. (2007). Central efferent pathways mediating skin cooling-evoked sympathetic thermogenesis in brown adipose tissue. *Am. J. Physiol. Regul. Integr. Comp. Physiol.* **292**, R127–R136.

Osborne, P. G., Sato, J., Shuke, N. and Hashimoto, M. (2005). Sympathetic α-adrenergic regulation of blood flow and volume in hamsters arousing from hibernation. *Am. J. Physiol.-Regul. Integr. Comp. Physiol.* **289**, R554–R562.

Payne, A. P. (1994). The harderian gland: a tercentennial review. *J. Anat.* **185**, 1–49.

Pengelley, E. T. and Fisher, K. C. (1961). Rhythmical arousal from hibernation in the golden-mantled ground squirrel, Citellus lateralis tescorum. *Can. J. Zool.* **39**, 105–120.

Porter, W. R. and Witmer, L. M. (2016). Avian Cephalic Vascular Anatomy, Sites of Thermal Exchange, and the Rete Ophthalmicum. *Anat. Rec.* **299**, 1461–1486.

Prakash, K. N. B., Verma, S. K., Yaligar, J., Goggi, J., Gopalan, V., Lee, S. S., Tian, X., Sugii, S., Leow, M. K. S., Bhakoo, K., et al. (2016). Segmentation and characterization of interscapular brown adipose tissue in rats by multi-parametric magnetic resonance imaging. *Magn. Reson. Mater. Phys. Biol. Med.* **29**, 277–286.

Raimbault, S., Dridi, S., Denjean, F., Lachuer, J., Couplan, E., Bouillaud, F., Bordas, A., Duchamp, C., Taouis, M. and Ricquier, D. (2001). An uncoupling protein homologue putatively involved in facultative muscle thermogenesis in birds. *Biochem. J.* **353**, 441–444.

Rasmussen, J. M., Entringer, S., Nguyen, A., Erp, T. G. M. van, Guijarro, A., Oveisi, F., Swanson, J. M., Piomelli, D., Wadhwa, P. D., Buss, C., et al. (2013). Brown Adipose Tissue Quantification in Human Neonates Using Water-Fat Separated MRI. *PLOS One* **8**, e77907.

Reeder, S. B., Pineda, A. R., Wen, Z., Shimakawa, A., Yu, H., Brittain, J. H., Gold, G. E., Beaulieu, C. H. and Pelc, N. J. (2005). Iterative decomposition of water and fat with echo asymmetry and least-squares estimation (IDEAL): Application with fast spin-echo imaging. *Magn. Reson. Med.* **54**, 636–644.

Rothwell, N. J. and Stock, M. J. (1979). A role for brown adipose tissue in diet-induced thermogenesis. *Nature* **281**, 31.

Rowland, L. A., Bal, N. C. and Periasamy, M. (2015). The role of skeletal-muscle-based thermogenic mechanisms in vertebrate endothermy. *Biol. Rev.* **90**, 1279–1297.

Tattersall, G. J. (2016). Infrared thermography: A non-invasive window into thermal physiology. *Comp. Biochem. Physiol. A. Mol. Integr. Physiol.* **202**, 78–98.

Tattersall, G. J. and Milsom, W. K. (2009). Hypoxia reduces the hypothalamic thermogenic threshold and thermosensitivity. *J. Physiol.* **587**, 5259–5274.

Trayhurn, P. and Beattie, J. H. (2001). Physiological role of adipose tissue: white adipose tissue as an endocrine and secretory organ. *Proc. Nutr. Soc.* **60**, 329–339.

Walker, R. (1958). Age changes in the rat's exorbital lacrimal gland. *Anat. Rec.* **132**, 49–69.

Wang, L. C. H. (1979). Time patterns and metabolic rates of natural torpor in the Richardson's ground squirrel. *Can. J. Zool.* **57**, 149–155.

Watanabe, M. (1980). An autoradiographic, biochemical, and morphological study of the Harderian gland of the mouse. *J. Morphol.* **163**, 349–365.

Weng, K. C. and Block, B. A. (2004). Diel vertical migration of the bigeye thresher shark (Alopias superciliosus), a species possessing orbital retia mirabilia. *Fish. Bull.* **102**, 221–229.

382 **FIGURES**

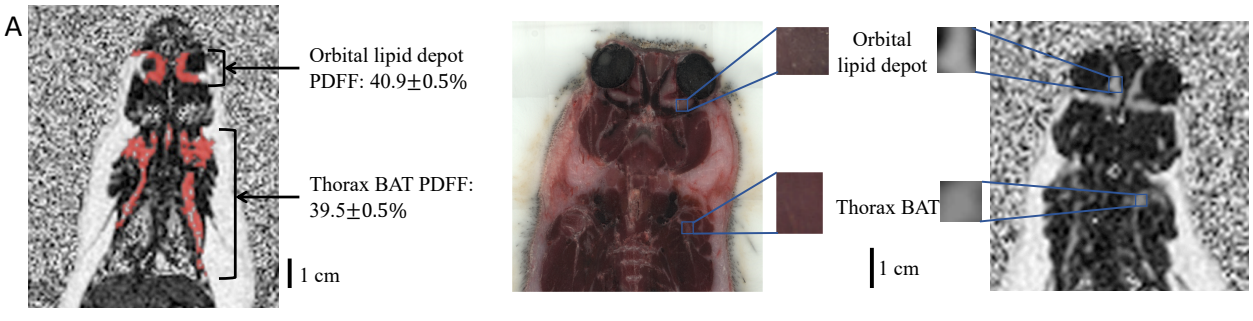

383

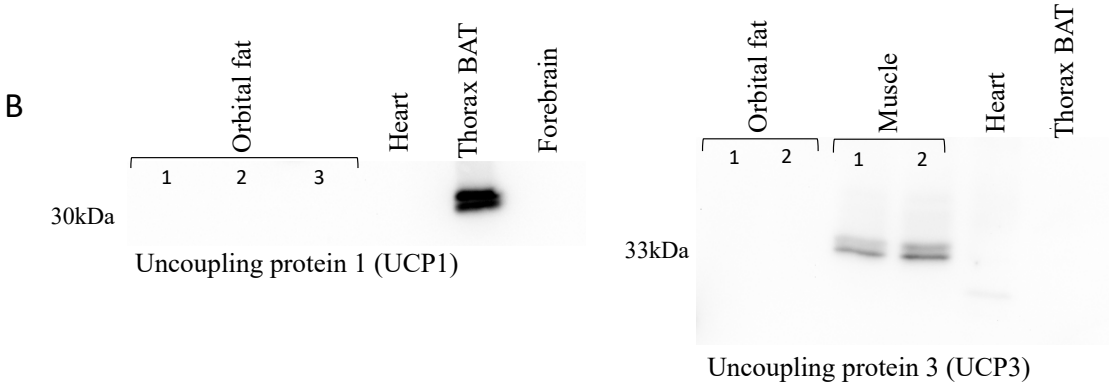

384

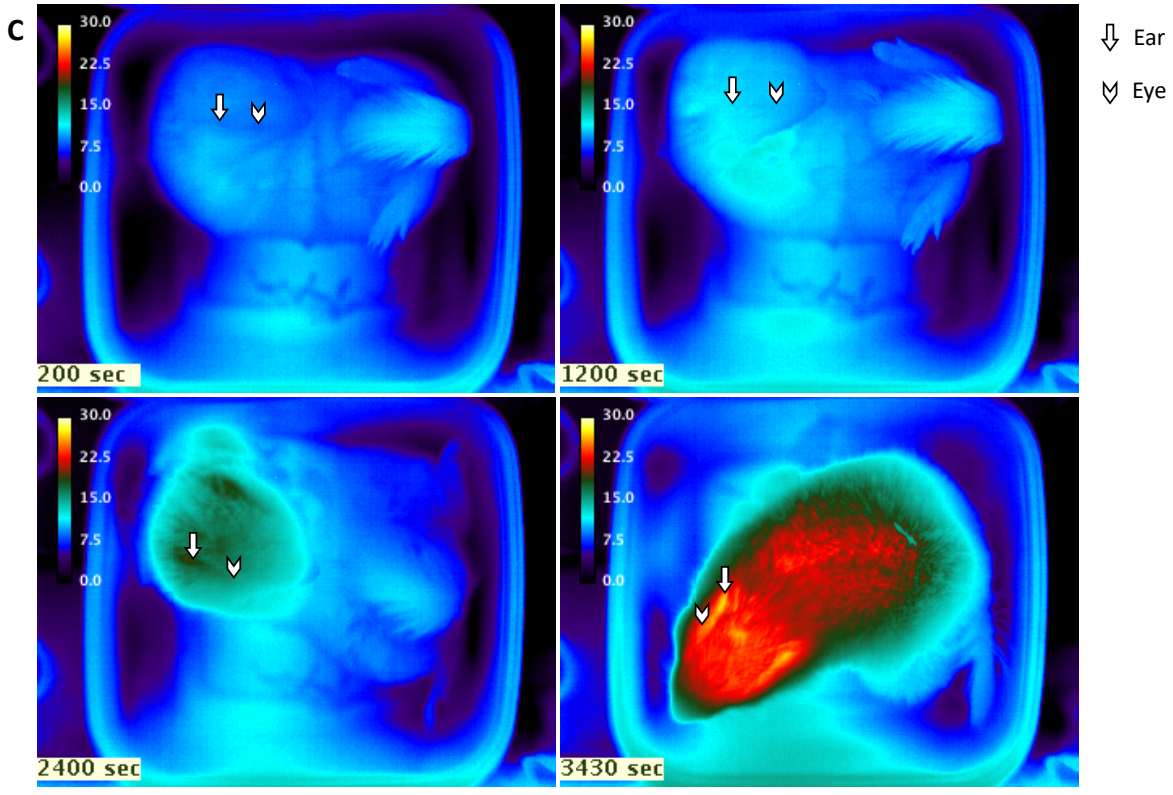

385

Figure 1 A) Proton density fat fraction (PDFF) magnetic resonance image (MRI) of a ground squirrel and CryoViz image of thorax. One example (left) of an MRI slice from a hibernating ground squirrel. Areas highlighted in red indicate location of PDFF values between 30–70%, expected values for BAT. The CryoViz image (center) shows that the orbital lipid depot corresponds precisely with the position of the tissue used for MRI analysis (right) and visual resembles it closely. **B) Immunoblots of uncoupling protein 1 (UCP1) and uncoupling protein 3 (UCP3) from various tissues of 13-lined ground squirrels**. Numbers indicate different individuals from which the orbital lipid depot or skeletal muscle was sampled**. C) Thermal images of a squirrel during an induced arousal.** Arrow head indicates approximate location of the eye and the arrow indicates approximate location of the ear. The top left image was taken 200 seconds after arousal was induced, the top right image was taken after 120 seconds, the bottom left image taken 2400 seconds and the bottom right images taken 3430 seconds after arousal was induced.

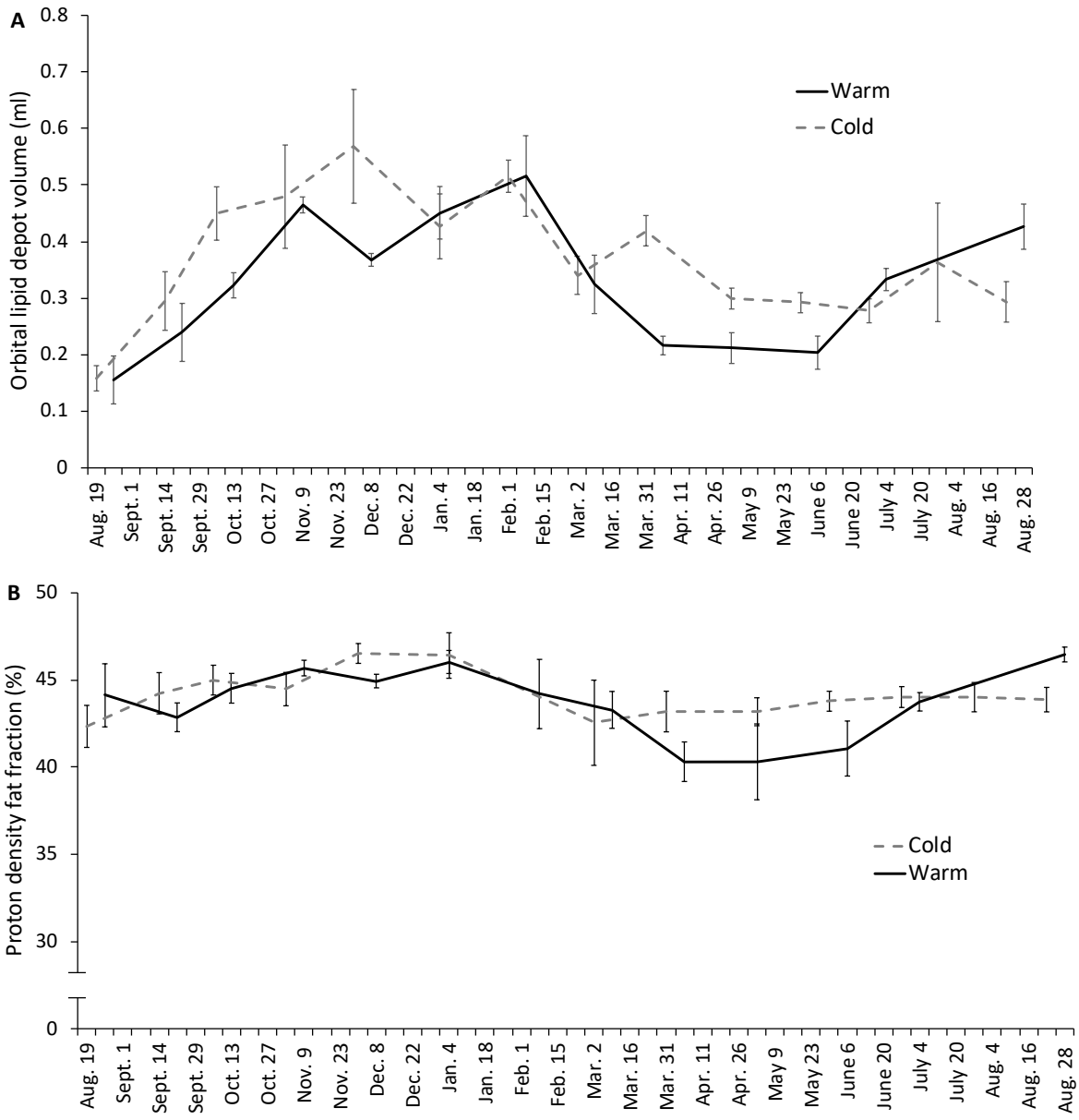

Figure 2 Volume of the orbital lipid depot over an entire year (A) and corresponding proton density fat fraction (PDFF) (B). The solid (–) line represents animals housed at 25°C and the dashed (--) line represents animals housed at 5°C. Both groups had a 12h L:12h D photoperiod. Data are presented as mean ± SE, $n = 4$ for each group. Repeated measures ANOVA for eye fat volume: effect of time ($F_{(3.0, 18.2)}$=10.9, P<0.001), temperature ($F_{(1, 6)}$=1.7, P=0.25) and interaction between time and temperature ($F_{(3.0, 18.2)}$=2.4, P=0.11). Repeated measures ANOVA for PDFF: effect of time ($F_{(2.6, 15.5)}$=3.7, P=0.051), temperature ($F_{(1, 6)}$=0.3, P=0.6) and interaction between time and temperature $F_{(2.6, 15.5)}$=1.5, P=0.3)

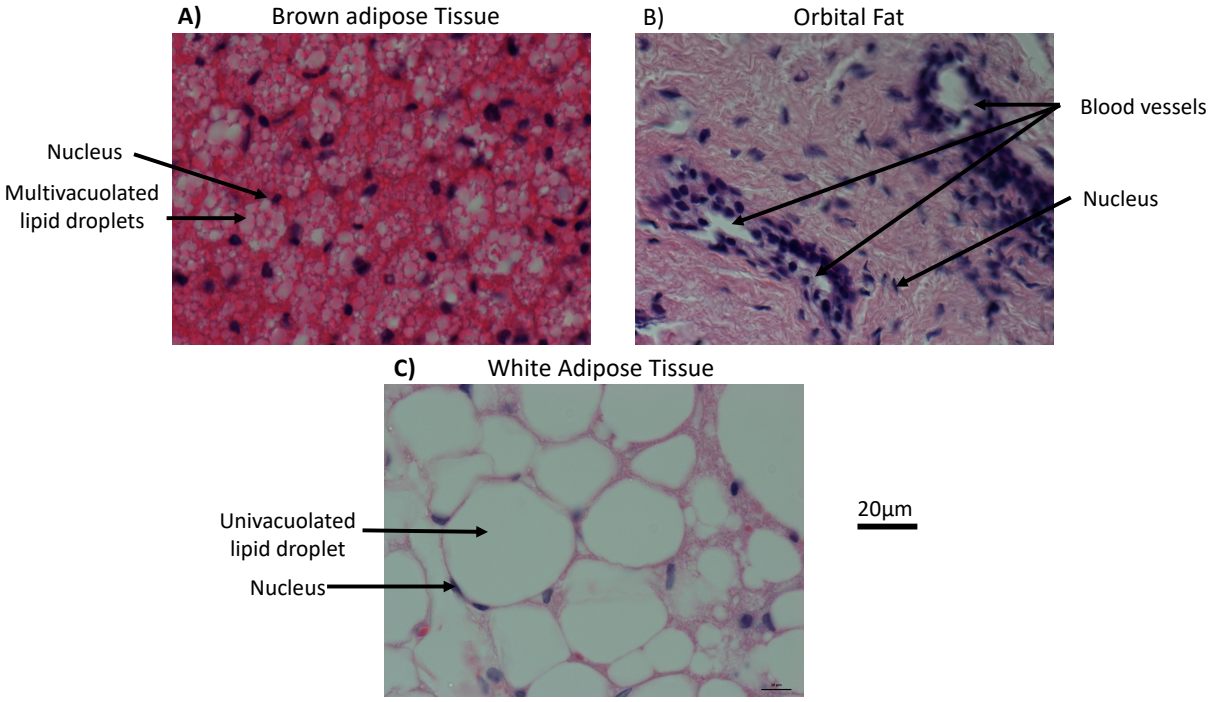

427

428 **Figure 3 Hematoxylin & Eosin staining of tissues.** Tissues were formalin fixed and paraffin
429 embedded. Sectioning shows distinct variations in histology of the tissues. All photomicrographs
430 are shown with the same magnification, scale bars indicate 20µm.
431